Failure prediction of a new sandwich panels based on flax fibres reinforced epoxy bio-composites

Frederic Lachaud, Mathieu Boutin, Christine Espinosa, David Hardy

Version of Record: https://www.sciencedirect.com/science/article/pii/S0263822320332876
Manuscript_a46cc81e07b4774be53babc33d781bd3

Failure prediction of a new sandwich panels based on flax fibres reinforced epoxy bio-composites

Frederic Lachaud[a*], Mathieu Boutin[a,b,c], Christine Espinosa[a], David Hardy[c]

[a] Institut Clément Ader (ICA), Université de Toulouse, CNRS UMR 5312-INSA-ISAE-Mines Albi-UPS, Toulouse, France

[b] Laboratoire de Chimie Agro-industrielle, LCA, Université de Toulouse, INRA, Toulouse, France

[c] VESO concept, 1620 Route de Bellevue 31530 Mérenvielle

*To whom correspondence should be addressed: Tel. +33561338568, E-mail: frederic.lachaud@isae-supaero.fr

Abstract

Flax fibres reinforced polymer composites are more and more used in various fields such as transportation due to the low density of flax paired up with good mechanical properties. This calls for a better understanding and prediction of the mechanical behaviour of such composites. In this study, the mechanical behaviour of flax fibres fabric reinforced polymer composites has been studied experimentally and numerically for composite laminates and for Omega stiffened Sandwich Panels. Composites laminates plies exhibited a strong non-linear mechanical behaviour due to the particular structure of flax fibres which is investigated. Likewise, the omega sandwich panels presented the same behaviour and high strength making them competitive with conventional glass fibres reinforced polymer composite sandwich panels used in aeronautics. A material model is proposed to describe the four phases non-linear behaviour that has been implemented to get a predictive finite element model (FE) .Different damage laws have been identified calibrated and implemented as a UMAT routine

to get a predictive finite element model (FE). The composite flax ply model includes diffuse damage, failure damage and residual strain. The material model has been validated for many stacking sequences. The finite element model including the four phase behaviour up to damage and failure is demonstrate to reproduce the crack locations and buckling zones and amplitudes of the omega panel under tension and three points bending.

Keywords: *Flax Fibre, Bio-composite, Composite laminate, Woven composite, Stiffness composite panel, Failure model, Damage model, Debonding, Cohesive zone model, 3 point bending,*

NOMENCLATURE AND UNITS

a^2	coupling pseudo-plastic parameter
b	coupling diffuse damage parameter
d_{dij}	diffuse damage parameter in ij directions
d_{fij}	failure damage parameter in ij directions
δ	displacement (mm)
Δa	crack length (mm)
E_{ij}	laminate Young's modulus (MPa) in ij directions
ε_{ij}	strain component in ij directions
ε_{eij}	elastic strain component in ij directions
ε_{pij}	residual strain component in ij directions
ε_{tij}	total strain component in ij directions
σ_{ij}	stress component in ij directions
σ_{eq}	Von Mises equivalent stress
Y_{ij}	elastic energy in ij directions
F	maximum strain at failure, failure strain criterion
Fp	pseudo plasticity yield function
G_{ij}	laminate shear modulus (MPa) in ij directions
Gf	critical energy release rate (J/m²) in axial warp/weft direction
Gm	critical energy release rate in mode II (J/m²) for matrix
lc	characteristic length (mm)
p	cumulative plastic strain
R	experimental hardening curve for isotropic hardening plasticity
R_0	experimental yield stress

3PB	three points bending
CZM	Cohesive Zone Model
FEM	Finite Element Method
FOSP	Flax fibre Omega Sandwich Panel

1. Introduction

Composites materials using natural fibres such as flax are increasingly studied in the aeronautic area due to their specific properties. Indeed, these fibres present high mechanical properties paired up with a lower density than classical glass fibres [1,2]. Wambua and al. [3] compare tensile and impact behaviour of short fibres composite materials (random mat form) realized with five types of natural fibres. It appears that the natural fibre composites tested were found to compare favourably with the corresponding properties of glass mat polypropylene composites. With this mind, such fibres could be beneficial for air transportation as long as their lower mass could allow a reduction in fuel consumption inducing lower costs and environmental impact. Another recent application of natural fibres is also their use for making honeycomb cores and may be replace Nomex® or Aluminium material. Riccio and al. [4] use flax fibres with thermoplastic resin to create honeycomb core for impact applications. Despite of that, flax fibres can be challenging to use as replacement for synthetic fibres in composite materials for different reasons [5]. First of all, the properties of these fibres strongly depend on the climatic condition of the plant culture and this phenomenon can lead to an important variability over years or geographical production areas which can become an issue in providing a consistent production quality to the industry [1,2,6]. Then, the adhesion between such fibres and most polymeric matrices is generally poor due to the incompatibility of the hydrophilic characteristic of natural fibres [7–9]. Usually, chemical or physical treatments are used to modify the fibres' surface and improve adhesion between the fibres and the matrix which is a cause of environment or cost effectiveness and competitiveness reduction [10–15]. In addition, natural fibres have a complex microstructure compared to synthetic ones [16–18]. Flax fibres are composed of concentric layers of different structures and compositions of cellulose, hemi-cellulose and lignin, and can be

considered as a composite at a lower scale as well. For example At a larger scale, flax fibres are discontinuous and have kink bands that can affect their mechanical response [19]. From a microscopic point of view, Baley [20] indicate that an increase of the Young's modulus is due to the reorganisation of the cell structure; especially reorientation of the fibrils toward the load direction. All these characteristics induce a nonlinear mechanical behaviour under loading along the direction of the fibres. Moreover, this nonlinear behaviour is observed in composite materials using this kind of fibres [21]. Finally, composite laminates made from flax fibres are subject to complex different damage mechanisms due to their structure and poor adhesion with polymeric matrices [22].

In order to predict the behaviour of composite materials, the Finite Element Method (FEM) is more and more used. FEM is efficient and convenient, compared to experimental methods, to study the behaviour of fibres and their composites or laminates. This method allows studying the influence of several parameters such as layers configuration, fibres volume fraction or mechanical properties of the fibres. Even if flax fibres have been well studied during the past decades, their mechanical characterization is not easy. The main difficulty is that these fibres do not present a linear behaviour even at low charges, in other words, their stiffness matrix is not constant throughout the loading phase. This particular nonlinear mechanical behaviour is challenging when it comes to model the homogenised composite materials compared to synthetic fibres composites such as carbon fibres' ones which exhibit a linear behaviour. Different FE models have been used to try to model the complex behaviour of natural fibres, or have been built to predict the behaviour of flax fibres at different scales. One of the most popular is going through a Representative Volume Element (RVE) that allows to take into account the microscopic heterogeneities of the fibres [23]. Thuault et al. [24] have designed another micro-scale FE model which takes into account the chemical components, the cell wall thickness and the micro fibrils angle to model the tensile behaviour. Other models have

been created at meso-scale like the one of Beakou and Charlet [25] based on the flax fibres bundles and the cohesive behaviour between fibres. At a larger scale, a FE model has been developed by Tephany et al. [26] for woven flax fabrics in 2D to model the influence of non-linear tensile behaviour of woven fabric. For the behaviour of composites reinforced with natural fibres, Sliseris et al. [27] have established a 3D RVE model for woven fibre fabric reinforced composite for the tensile and shear properties of composites using non-linear plasticity model. Finally, damage and fracture have been modelled for woven fabric reinforced composites in 2D using shell elements by Wang et al. [28] and in 3D using a meso-scale RVE model by Panamoottil et al. [29]. But there is not one unique FE model or behaviour law that takes into account all the previously described characteristics.

The main objective of this study is to propose a meso-scale damage behaviour model capable to replicate the non-linear behaviour of flax/epoxy composites and complex structures. It is demonstrated that this model is capable to predict the damage and failure of a flax fibres reinforced composite omega sandwich panels which are complex structures. Omega stiffeners are often used to improve the compressive strength of composite panels [30]. For our study the Omega stiffeners are used to replace the Nomex® core in our sandwich panels.

To do so, mechanical behaviour of flax fibres composites and associated panels have been experimentally studied. The performance of Flax fibre Omega Sandwich Panels to a three points bending load is compared with classical Nomex® Core sandwich panels. Then, the results of these tests and the damage laws have been identified in order to implement the FE model. Finally, the model has been used to predict the behaviour of the composite panel structure and compared to experimental results.

2. Materials and Experimental Protocol

2.1. Flax fabric Composite Laminates behaviour

2.1.1. Manufacturing

Composites laminates were manufactured using a twill 2/2 woven flax fibres fabric provided by Groupe Depestele (Le Bocasse, France), having an area weight of 360 g/m^2. The matrix used was composed of the SR-1126 resin and SD-8202 hardener provided by Sicomin (Châteauneuf les Martigues, France). Sample plates were manufactured by compression moulding with four layers of flax fibres fabrics soaked with a weight mix ratio of resin and hardener of 100:22 for 1h under 10 bars at 100 °C. The measured fibre volume fraction of 40% was estimated from the difference between the weight of the composite and the weight of used fibres. Three specimens for each configuration of 200mmx25mm were cut in the plates and prepared for tensile tests (Figure 1). Thickness of all the samples is 2.5 mm. One mm thick woven fiberglass laminated tabs are bonded to the specimens for introduction of the load by the tensile machine. Specimens were manufactured in order to get different configurations of load to the weft/warp directions, namely $[0°]_4$, $[90°]_4$ and $[\pm45°]_4$ in order to study the behaviour of the laminate.

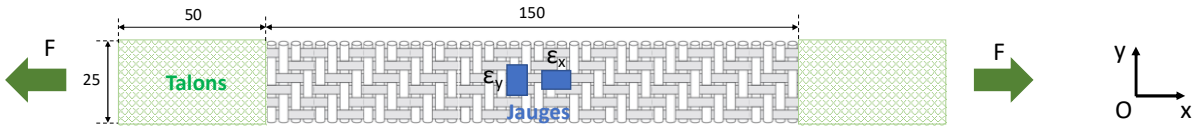

Figure 1: Tensile Stress-Strain behaviour of $[0]_4$ samples

Tensile tests were performed using an Instron model 8862, in accordance with ASTM D3039 / D3039M - 17 standards.

2.1.2. Experimental results

This part is intended to explain the static analysis that has been carried out in order to derive the model of the behaviour and for the damage. For this late case, a cyclic tensile test is necessary.

First, in order to understand how this damage is acting, a real cyclic tensile test has been conducted in the laboratory on the previously described specimens, so that to create loads in several directions from the fibres' ones. This directions were: the direction taken as reference (0°), also called warp, the direction perpendicular to this one (90°), also called weft, and a (45°) direction for the first one, in order to measure the in-plane/in-ply shear stress.

For the sake of clarity, two of the three stress-strain curves obtained for the $[0°]_4$ configurations are presented on Figure 2. As expected from literature, the mechanical behaviour of flax fibres woven composite coupons is non-linear and exhibits three different stages. This particular behaviour begins with a small linear phase up to 0.2 % of total engineering strain. Then, there is a long non-linear hardening phase up to around 1.2%-1.4 % of total strain. Finally, the failure of the specimens is observed at 1.4 % of total strain. As expected, the mechanical behaviour of the $[90°]_4$ specimens was nearly the one of the $[0°]_4$ ones. The curves are not reported here for the sake of simplicity and because of their similarity with Figure 2.. Resultant mechanical properties are presented in Table 1. This observation is consistent with the fact that in an equilibrated fabric, the behaviour is the same in both in-plane directions.

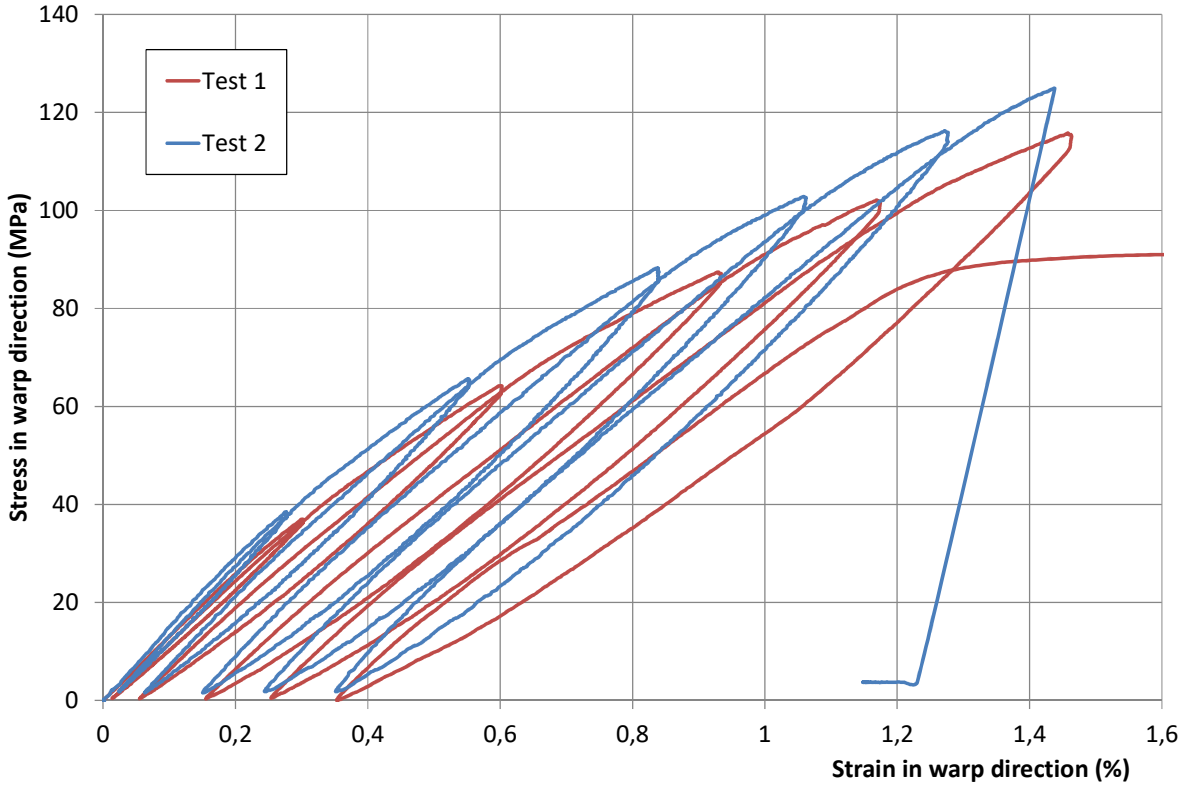

Figure 2 : Tensile engineering Stress-Strain behaviour of $[0°]_4$ samples

The failure surfaces from a typical (0°) test are shown in Figure 3. The analysis of these pictures shows a clear fracture of the fibres located between two yarns in the direction perpendicular to the direction of loading. Moreover, some fibres seem to have slipped in the composite.

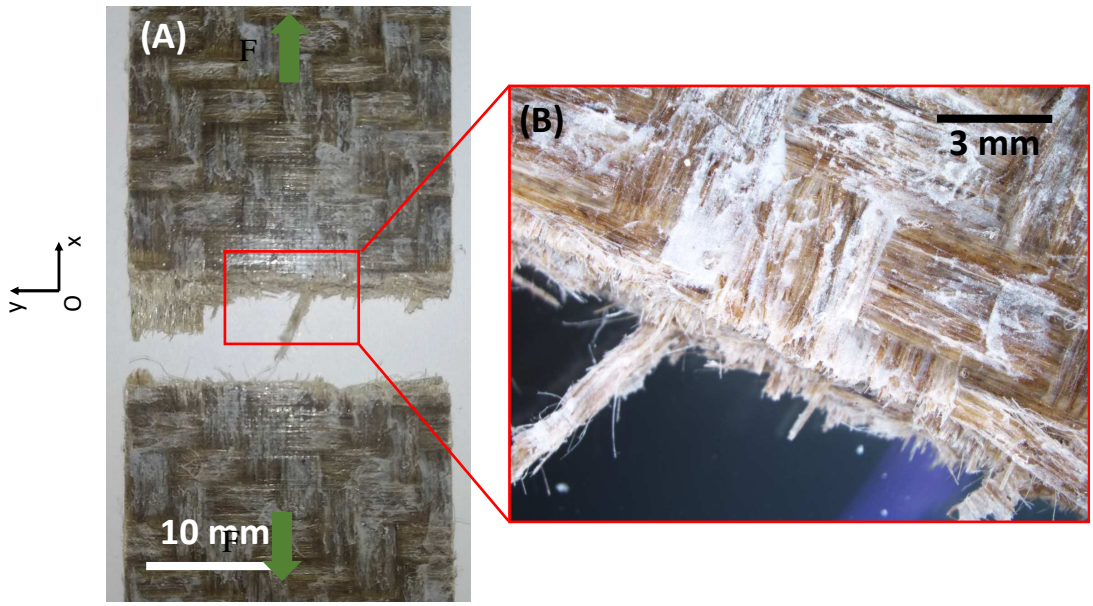

Figure 3 : Failure profiles of the $[0°]_4$ samples under cyclic tensile load

The analysis of the curves and of the fracture surfaces shows the appearance of damage during tensile tests responsible for the non-linear behaviour of the composite. Such behaviour is mainly due to flax fibres because of two effects. On the one hand, the particular structure of flax fibres changes during loading. O the other hand the woven pattern is composed of long fibres that are indeed discontinuous and simply stuck together. Therefore they can easily slip and slide on each other. Moreover, the adhesion between the fibres and the matrix may not be perfect.

The curves corresponding to the in plane shear stress as a function of the total engineering strain for the $[\pm 45°]_4$ configurations are shown in Figure 4. In this case, the non-linear mechanical behaviour is slightly different. The first linear phase is longer and goes up to 1 % of deformation. Then, the non-linear part continues up to around 6 % of deformation. The decrease of the stiffness slope in this case is very significant. The different mechanical properties measured with this test are presented in Table 1.

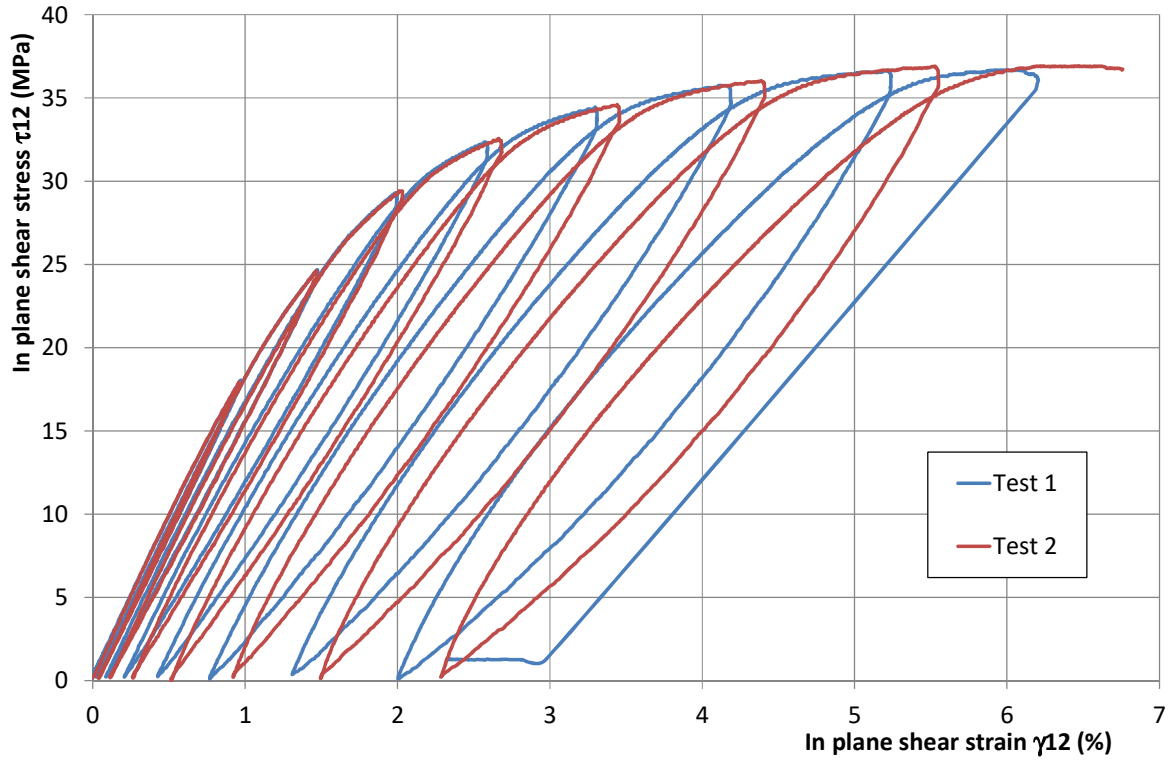

Figure 4 : In plane shear Stress-Strain behaviour of $[\pm 45°]_4$ samples

The pictures of the fracture surfaces of the $[\pm 45°]_4$ configuration are presented in Figure 5. Two different phenomena can be observed on these pictures. First, the different yarns composing the fabrics have slipped between each other as it can be seen in Figure 5-A. Such behaviour is normal in this kind of configuration. On Figure 5-B-C, it can be seen that there are some fractures of the fibres that were not expected.

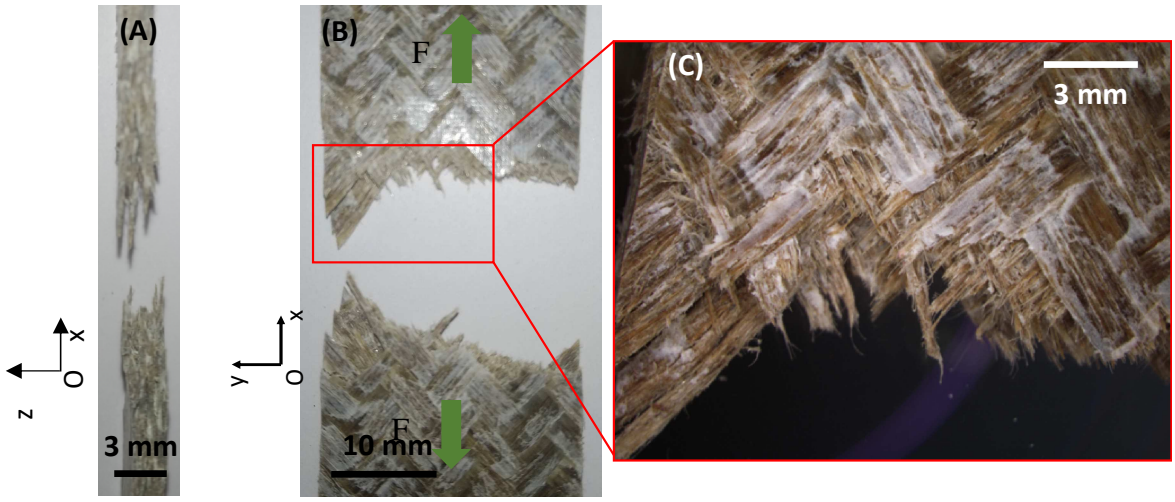

Figure 5: Failure profiles of the [±45°]$_4$ samples under cyclic tensile load

The decrease of the slope of the curves for the [±45°]$_4$ configuration can be explained by the fact that in this configuration, the tensile tests do not strain the fibres but rather the matrix that is weaker. Furthermore, the non-perfect adhesion between the fibres and the matrix contributes to the initiation and final shape of the damage.

In the following Table 1, E_0 stands for the apparent elastic modulus during the elastic phase; σ_{max} and ε_{max} are respectively the maximum reached values of engineering axial stress and strain. The Poisson ratio is computed using the ratio of measured lateral to axial strains.

Table 1: Young's moduli and failure characteristics of flax fabric ply

Laminate	E_0 (GPa)	σ_{max} (MPa)	ε_{max} (%)	ν
[0°]	13.9 ± 0.5	122 ± 0.2	1,37 ± 0,21	0,13
[90°]	14.0 ± 1.2	121 ± 6.0	1,45 ± 0,01	0,10
±[45°]	2.1 ± 0.2	36 ± 0.3	6,48 ± 0,39	-

2.2. 3 points bending Omega Sandwich Panels behaviour

2.2.1. Manufacturing

Corrugated panels were manufactured using the same products as used for composite laminates. The core and the skins were made separately using only one layer of flax fibres fabric, while the omega stiffeners are made from four layers as for the tensile specimens. The manufacturing process of the skins was the same as the one used for composites laminates (except for the number of layers). The core was manufactured using a special aluminium mould that has been designed and manufactured in purpose so that to obtain the specific required omega shape of the core. The curing pressure and temperature used were the same as previously mentioned. The core and the skins were then assembled using the matrix as the adhesive. Once assembled, the panel was post cured for 1 h at 100 °C in an oven. The rendering aspect of the panels and the 200mmx80mmx10mm specimens that were cut from them and used for flexural tests are shown in Figure 6.

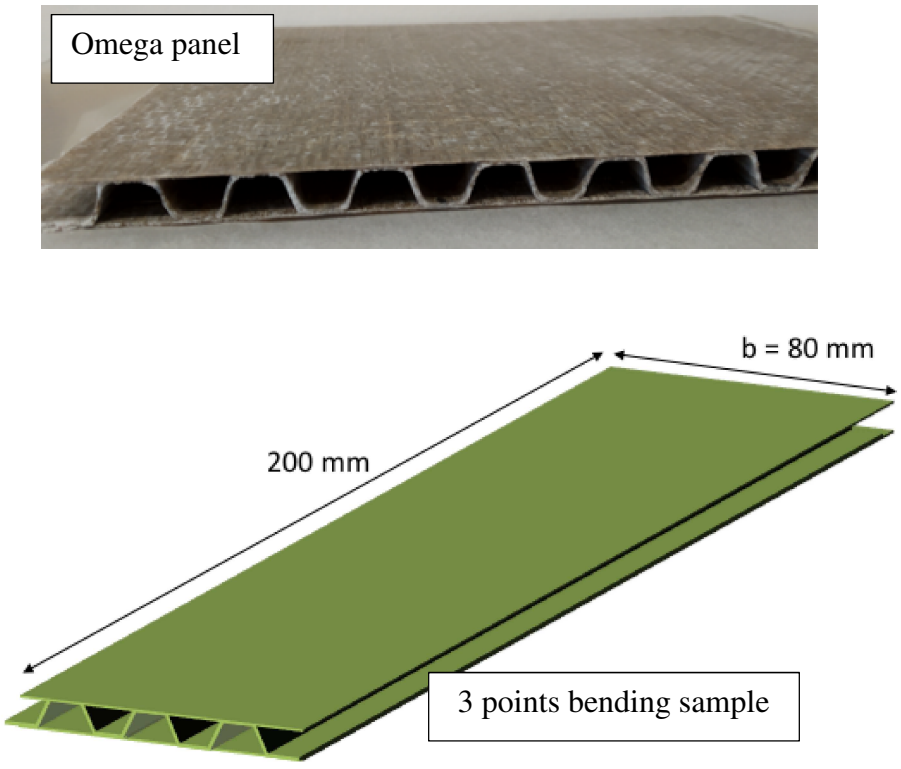

Figure 6: Flax fibres Omega panels and 3 points bending specimen dimensions

2.2.2. Experimental results

Omega sandwich panels were submitted to three point bending tests as described on Figure 8. Tests were conducted using a 10 KN INSTRON® tensile machine. The sample is set on two rollers to let free the in plane movement, which relative distance is 150 mm. A wedge has been introduced under the central roller to minimize the crushing effects of the upper skin of the panel.

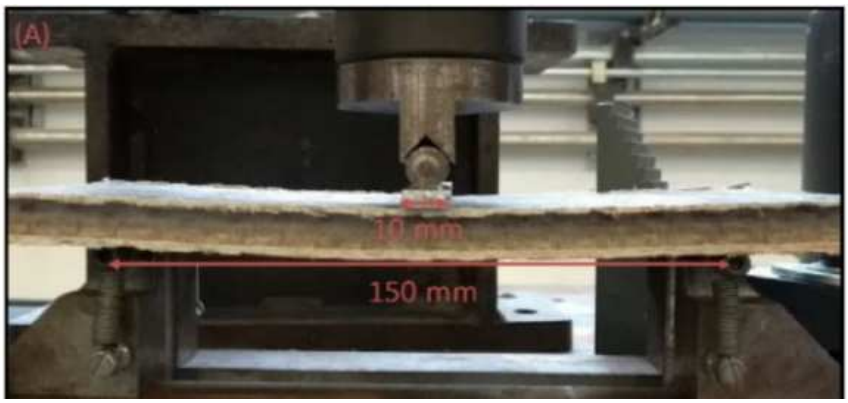

Figure 7: 3 points bending test setup

A prescribed displacement is applied to the upper roller with a speed of 1 mm/min.

In order to compare our Omega sandwich panel to classical aeronautical aircraft cabin panel, we used also Glass Fibre / NOMEX sandwich panel during test campaign. These sandwich panels were supplied by Norbond© (NORDAM® reference, 0.5 inch thick, NB220-0155-500B). The thickness of these panels was *c*hosen closest to Omega flax fiber sandwich panels so as to obtain an almost identical basis weight.

Measured load versus displacement is shown Figure 8. Like the flax fibres composites laminates, the omega sandwich panels present a non-linear behaviour with three phases. Two different behaviours appear, or more precisely two rupture modes, for the omega sandwich panels. The first one, represented by continuous blue lines exhibits a clear fracture at 7 mm of displacement with a higher maximal load of 2250 N. The second one, represented by dashed blue lines, presents a softer fracture or may be a succession of smaller fractures with a lower maximal load of 1960 N. Furthermore, flax panels exhibit comparable load sustainability in

comparison to classical glass fibres – epoxy/Nomex® sandwich panels, with a higher deformation to failure. This shows the potential of such structure made of natural fibres. The mechanical properties of panels are compared in Table 2.

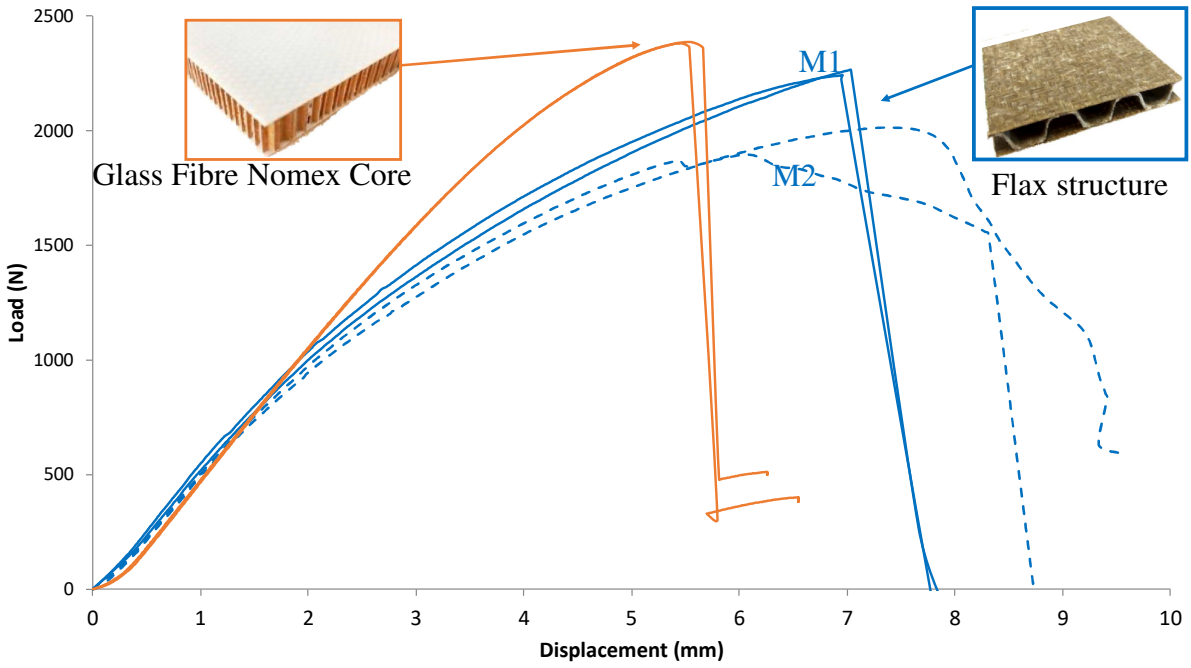

Figure 8: Load displacement behaviour comparison of omega sandwich panels and a commercial Glass fibres/Nomex® sandwich panels

Table 2: Comparison of characteristic behaviour of Flax Omega panels and Glass Nomex Panels(M1: failure mode 1, M2 failure mode II)

Panel type	Thickness (mm)	Surface weight (kg/m^2)	Force at Failure (N)	Stiffness (N/mm)	failure Force per surface weight (N/kg.m^2)
Glass fibres / NOMEX	12.70	2.9	2353	562	811
Flax fibres OMEGA M1 (mean)	11.27	3.1	2250	577	658
Flax fibres OMEGA M2 (mean)	11.27	3.1	1845	577	658

The fracture areas of the two fracture modes (M1 and M2) observed are shown in Figure 9. The Figure 9-A shows the fracture of the specimens with a clear fracture and high load. A lower skin tensile and core fracture can be seen on the picture. The Figure 9-B shows the buckling of the upper skin under compressive mode for the specimens with the lowest maximal load. This

difference of mode of rupture may result from some defects during the processing of the panels, particularly during the phase of bonding of the core and the skins.

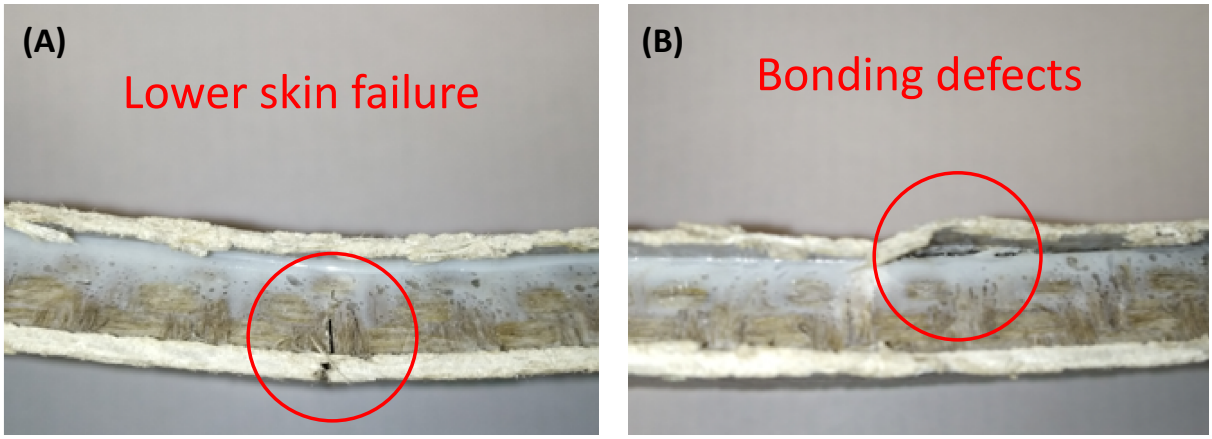

Figure 9: Omega sandwich flax panel failure, A) Failure mode 1 M1, B) Failure mode 2 M2

3. Flax ply Damage / Failure Model

The previous observations are used to propose hereafter a behaviour law, starting from a 1D description up to a full 3D model.

3.1. 1D damage/failure behaviour

In order to define in a simple form the variables of our behaviour model, we present first a 1D version on Figure 10. The 3D model will be described in the next section following the same 1D base model formalism. Observing the global behaviour of flax fabric composite ply under tensile test Figure 2 and Figure 4 for example, we can define three plus one behaviour phases:

- The first one is a linear elastic part up to a stress yield called Ro,
- The second one starting from Ro corresponds to a hardening behaviour where damage increases in a stable development process,
- The third one starting at the maximum load level describes a softening behaviour where failure occurs,

- Residual strain can be observed if load-unload are realized, so a fourth part can be considered.

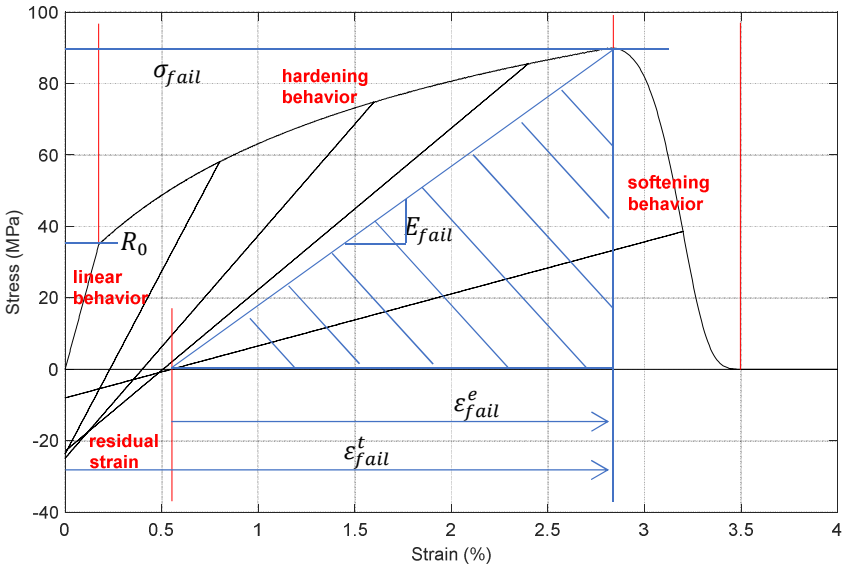

Figure 10: Example of a typical damage/failure behaviour

In order to model this behaviour in 1D, each phase is attributed a specific parameter and so a specific theoretical approach. The stress-strain 1D behaviour can be written as follows:

$$\sigma_e = (1 - d_d)(1 - d_f)E_0(\varepsilon_t - \varepsilon_r) \qquad \textit{Eq. 1}$$

Linear phase:

The first linear phase corresponds to a classic linear elastic behaviour defined by the Young modulus E_0. The hardening behaviour is due to a stable damage development composed of micro-cracks occurring all over the sample volume. This stable damage is named diffuse damage d_d. The softening behaviour is defined by the failure damage variable d_f. Finally, the permanent or residual strain ε_r can be computed and subtracted from the total strain ε_t value in order to compute the relaxed elastic strain value by the classical sum approach valid

if strains remain relatively small. So the initial stiffness is affected by both diffuse damage and failure damage. The derivation of each damage variable is described hereafter as follows.

Diffuse damage computation: thermodynamic approach:

For the hardening behaviour damages are due to micro-crack of the matrix but also due to micro-structure of flax fibres [31]. Flax fibres are made up of microfibrils which slide relatively to each other during tensile loads. Micro friction arrives between microfibrils that explains residual strains and permanent damages. The multiscale structure (multi cell wall) of these fibres contributes also to create damage.

According to thermodynamic approach [32], diffuse damage is written as a function of elastic energy Y:

$$d_d = f(Y) \qquad \textit{Eq. 2}$$

Where :

$$\mathrm{Y} = \frac{1}{2} E \epsilon^2 = \frac{1}{2}\frac{\tilde{\sigma}^2}{E_0} = \frac{1}{2}\frac{\sigma^2}{E_0(1-d)^2} \qquad \text{is the elastic energy}$$

The function f will be determined experimentally.

Failure damage computation: Strain failure criterion approach:

Softening behaviour is modelled with a failure damage variable computes according a strain failure criterion as defined by Linde [33].

$$d_f = 1 - \frac{exp((1-F).E_{fail}.\left(\varepsilon^e_{fail}\right)^2.l_c./G)}{2.F} \qquad \textit{Eq. 3}$$

Where :

- F is a maximum strain criterion $F = \frac{\varepsilon_t}{\varepsilon_r}$ for a 1D example criterion,
- ε_{fail} is the total strain at failure determined experimentally
- ε^e_{fail} is the elastic strain at failure

- E_{fail} is the damaged Young's modulus for strain at failure
- G is the critical energy release rate (J/m2) determined experimentally
- lc is a characteristic length for a non-local approach (m) with FE use.

Lc value is computed by the software. We have modified a user routine in Abaqus in order to compute this length in the perpendicular direction of the yarns direction in order to be coherent with fracture mechanic theory.

Residual strain computation: isotropic work hardening pseudo plasticity approach:

Residual strain is computed according a classical plasticity theory with isotropic hardening hypothesis applied to composite laminates [32]. Plasticity is here called pseudo-plasticity because the physical phenomena involved in the generation of irreversible strains are not the same as in metallic materials which suffer from plasticity.

The pseudo plasticity yield surface is defined with a plasticity function *Fp* given by:

$$Fp(\tilde{\sigma}, p) = \tilde{\sigma}_{eq} - R(p) - R_0 \qquad \textit{Eq. 4}$$

The irreversible strain component linked to hardening computation is:

$$\dot{\varepsilon_p} = \dot{\lambda}\frac{\partial Fp}{\partial \sigma} = \dot{p}\frac{\sigma}{|\sigma|} \qquad \textit{Eq. 5}$$

For 1D approach and isotropic hardening $\dot{\lambda} = \dot{p}$, so the only value of residual strain is :

$$\dot{\varepsilon_p} = \dot{p}\frac{\sigma}{|\sigma|}$$

Where :

- $\tilde{\sigma}_{eq}$ is the equivalent effective stress (equal to $\tilde{\sigma}$ for 1D formulation),
- $R(p)$ is a function defining the hardening curve, determined experimentally,
- p is the cumulative plastic strain ($\lambda = p$) for isotropic hardening,
- R_0 is the pseudo-plastic yield stress determined experimentally.

For the formulation of each phase' behaviour, tests are necessary. The identification of all the parameters will be detailed in the following paragraphs. However, firstly, this model is generalized for a 2D approach for the ply in a 3D modelling purpose.

3.2. 3D behaviour: 2D in plane damage of the ply

For 3D generalization, the model includes a vector of three diffuse damages and a vector of three failure damages. Pseudo plasticity permits to compute also three in plane residual strains. So the model affects the in plane behaviour of the ply.

The stress-strain behaviour is written in a general form:

$$\{\sigma\} = [C_{\overline{\overline{D}}}].\{\varepsilon\} \qquad \textit{Eq. 6}$$

Where:

$$C_{\overline{\overline{D}}} = \begin{bmatrix} (1-D_{f1})(1-D_{d1})C_{11} & (1-D_{f1})(1-D_{f2})(1-D_{d2})C_{12} & (1-D_{f1})(1-D_{d2})C_{13} & 0 & 0 & 0 \\ C_{21} & (1-D_{f2})(1-D_{d2})C_{22} & (1-D_{f3})(1-D_{d2})C_{23} & 0 & 0 & 0 \\ C_{31} & C_{32} & C_{33} & 0 & 0 & 0 \\ 0 & 0 & 0 & (1-D_{f1})(1-D_{f2})(1-D_{f3})(1-D_{d3})C_{44} & 0 & 0 \\ 0 & 0 & 0 & 0 & C_{55} & 0 \\ 0 & 0 & 0 & 0 & 0 & C_{66} \end{bmatrix}$$

d_{di}, d_{fi} are the diffuse and failure damages in warp, weft and in plane shear directions respectively for i=1, 2 or 3.

The equivalent thermodynamic force to compute diffuse damages [32] is:

$$Y = \sqrt{b.(Y_{11} + Y_{22}) + Y_{12}} \qquad \textit{Eq. 7}$$

Where:

- Y_{ij} are the thermodynamic forces in warp, weft and in plane shear directions respectively,
- $b = \frac{G_{12}}{E_{11}}$ is a coupling parameter.

The failure damage variables' computation needs to introduce a strain criterion. The stress-strain criterion approach was proposed by [33] for unidirectional laminates. It is proposed here to adapt these criterions to the flax woven ply.

The warp direction failure criterion is computed as follows:

$$F_1 = \sqrt{\left(\frac{\varepsilon_{11}^2}{\varepsilon_{11}^{\text{Fail\_t}}\varepsilon_{11}^{\text{Fail\_c}}}\right)+\left(\frac{1}{\varepsilon_{11}^{\text{Fail\_t}}}-\frac{1}{\varepsilon_{11}^{\text{Fail\_c}}}\right)\varepsilon_{11}} > 1 \qquad \textit{Eq. 8}$$

The weft direction failure criterion is expressed by the criterion:

$$F_2 = \sqrt{\left(\frac{\varepsilon_{22}^2}{\varepsilon_{22}^{\text{Fail\_t}}\varepsilon_{22}^{\text{Fail\_c}}}\right)+\left(\frac{1}{\varepsilon_{22}^{\text{Fail\_t}}}-\frac{1}{\varepsilon_{22}^{\text{Fail\_c}}}\right)\varepsilon_{22}} > 1 \qquad \textit{Eq. 9}$$

The in plane shear failure criterion can be written as:

$$F_{12} = \sqrt{\left(\frac{\gamma_{12}}{\gamma_{12}^{\text{fail}}}\right)^2 + b\left[\left(\frac{\varepsilon_{11}^2}{\varepsilon_{11}^{\text{Fail\_t}}\varepsilon_{11}^{\text{Fail\_c}}}\right)+\left(\frac{\varepsilon_{22}^2}{\varepsilon_{22}^{\text{Fail\_t}}\varepsilon_{22}^{\text{Fail\_c}}}\right)\right]} > 1 \qquad \textit{Eq. 10}$$

Where :

$\varepsilon_{\text{ii}}^{\text{Fail\_t}}$ is the strain the failure in warp/weft direction in tensile

$\varepsilon_{\text{ii}}^{\text{Fail\_c}}$ is the strain the failure in warp/weft direction in compressive

$\gamma_{12}^{\text{fail}}$ is the shear strain failure in plane direction,

Finally, each failure damage variable can be computed by

$$d_f^i = 1 - \frac{exp((1-Fi).E_{fail}^i.\left(\varepsilon_{fail}^{e\,i}\right)^2.l_c./Gi)}{2.Fi} \qquad \textit{Eq. 11}$$

The equivalent stress introduced in the pseudo-plasticity yield function $Fp(\tilde{\sigma}, p)$ is:

$$\tilde{\sigma}_{eq} = \sqrt{a^2.(\tilde{\sigma}_{11}^2 + \tilde{\sigma}_{22}^2) + \tilde{\sigma}_{12}^2} \qquad \textit{Eq. 12}$$

Where:

- a^2 is a coupling parameter between residual strains

3.3. Identification of material parameters

The identification of the properties and parameters of the behaviour are done using tests in three steps. The first step permits to identify the Young's modulus, the strain at failure and the diffuse damage evolution.

This phase consists in realizing tensile tests for $[0°]_4$, $[90°]_4$ and $[\pm 45°]_4$ with loads-unloads cycles.

<u>Diffuse damage identification parameters</u>

First we assume that for a 2x2 twill fabric ply, behaviours according to warp or weft directions are the same. So only $[0°]_4$ test samples were used to identify diffuse damage and pseudo-plasticity parameters. The diffuse damage behaviour is identified with load-unload tests by measuring for each cycle, the modulus, the stress and total elastic values and the residual strains as shown Figure 11.

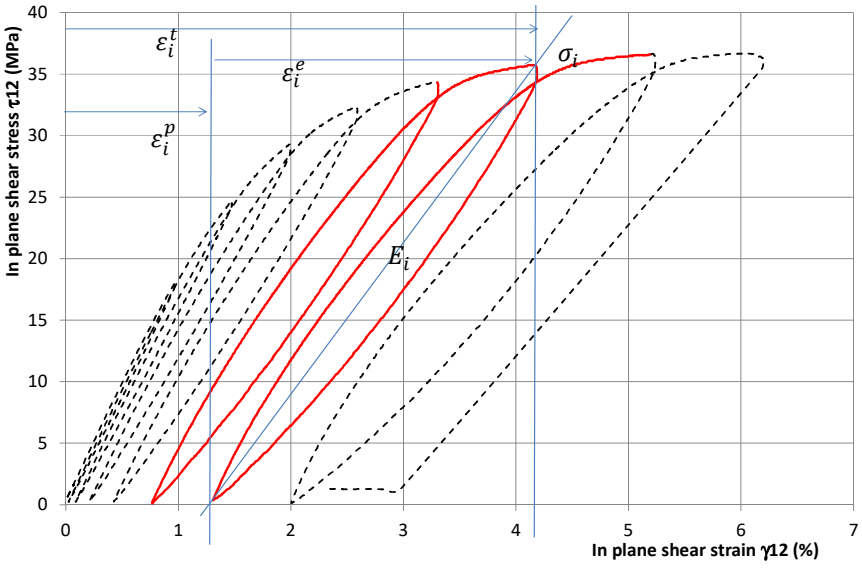

Figure 11: Example of damage parameters measurement on a $[\pm 45°]_4$ tensile test

And the damage can be expressed as:

$$d = 1 - \frac{E_i}{E_0} \qquad \textit{Eq. 13}$$

Therefore Y can be expressed too as:

$$Y = \frac{1}{2}\frac{\sigma^2}{E_0(1-d)^2} \qquad \textit{Eq. 14}$$

The identification method consists in determining the damage in the warp direction, then in in-plane shear direction. In fact, during the shear test, the yarns in the warp direction are stressed and the damage in shear must take this into account. Then the shear diffuse damage is corrected introducing non linear behaviour of the yarns in warp direction. Diffuse damage identification curves are plotted Figure 12.

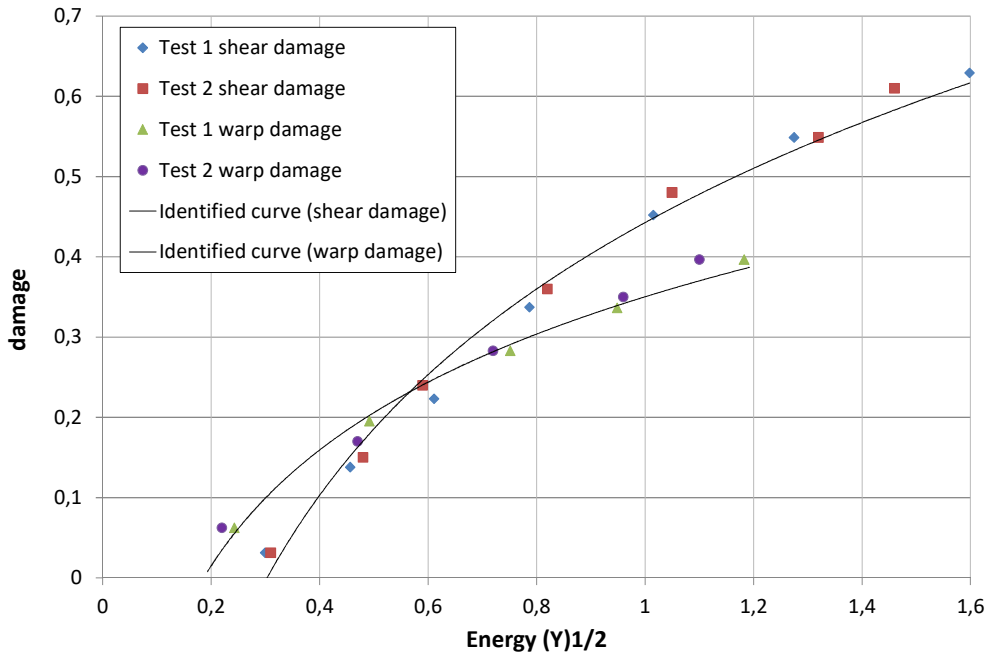

Figure 12: Diffuse damage identification curves

These curves follow a logarithm equation of the form d=A.Log(Y)+B. Non-dimensional constant values in both cases are given in Table 3.

Table 3. Identified values of diffuse damage

	A	B
±[45°]	0.3708	0.4427
[0°] & [90°]	0.2083	0.3503

Cumulative plasticity strain is defined by:

$$p = (1 - d).\epsilon_r \qquad \textit{Eq. 15}$$

Pseudo plasticity threshold is computed with:

$$R(p) + R_0 = \frac{\sigma_t}{(1-d)} \qquad \textit{Eq. 16}$$

As for damage identification, the methodology for plasticity identification consists in computing the residual strain versus yield stress for a $[0°]_4$ laminate. Then $[\pm 45°]_4$ laminate is used to find the yield stress versus the cumulative residual strain and also the coupling coefficient "a^2".

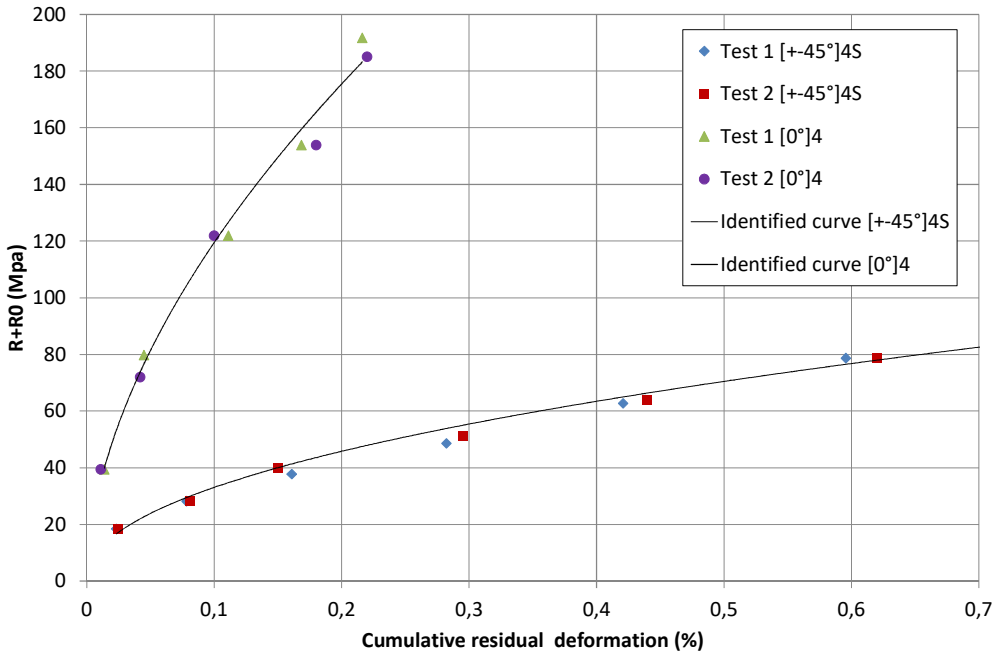

Figure 13: Pseudo-plasticity identification curves

These curves follow a power law of the form $R(p)+R_0=A.(p)^B$. Constant values in both cases are shown in Table 4.

Table 4. Identified values for pseudo plasticity

	A	B
±[45°]	97.6	0.471
[0°] & [90°]	428.3	0.554

a^2 is equal to 0.075 which means that the ratio between the residual strain in warp direction is about 13 times lower than that in in-plane shear.

For failure damage Eq. 3 needs to identify the critical energy release rate Gf for the fibres (warp and weft yarn direction) and Gm for the matrix. Compact Tension (CT) tests have been realized for yarns (warp and weft direction) Gf identification using the same samples as described by Pinho [34]. A precedent study [35] concerning 3D woven composites shows us that the area method is the more robust method to determine Gf. We use the same experimental approach to determine Gf in the warp direction of our flax woven composite. Dimensions of the sample are shown Figure 14a. Loading is shown on Figure 14b. A thick laminate$[0]_{12}$ is used in order to obtain about 4 mm thickness for the samples. The pre-crack has to be designed in order to be sure that the propagation is stable. A 6mm length has been chosen and is realized with a diamond wire.

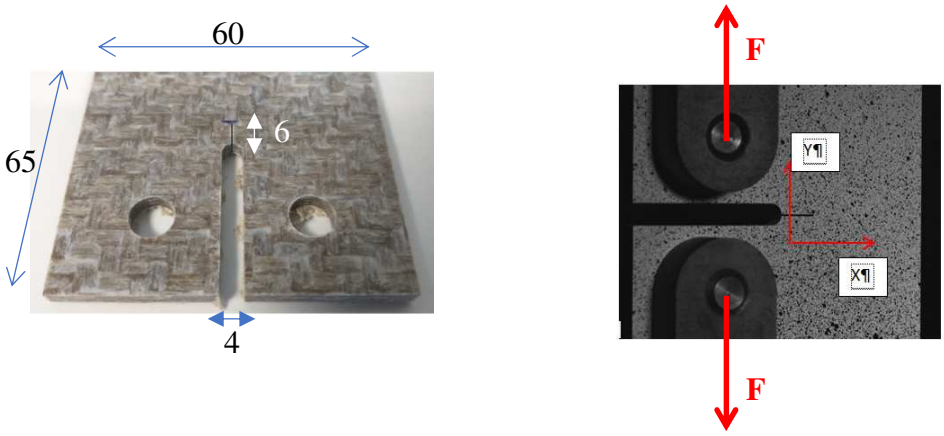

a) b)

Figure 14. CT sample dimensions (a) and tensile test configuration with DIC measurement (b)

Figure 15 presents typical load displacement curves for these tests.

The computation of the critical energy release rate Gf (J/m2) in warp and weft direction is calculated between two points (P1 and P2) on the path of the crack propagation. Critical loads and critical displacements for these two points together with the crack length measurement permit to compute G with:

$$Gf(0° \; or \; 90°) = \frac{P_1.\delta_1 - P_2\delta_2}{2.B.\Delta a} \qquad Eq.\ 17$$

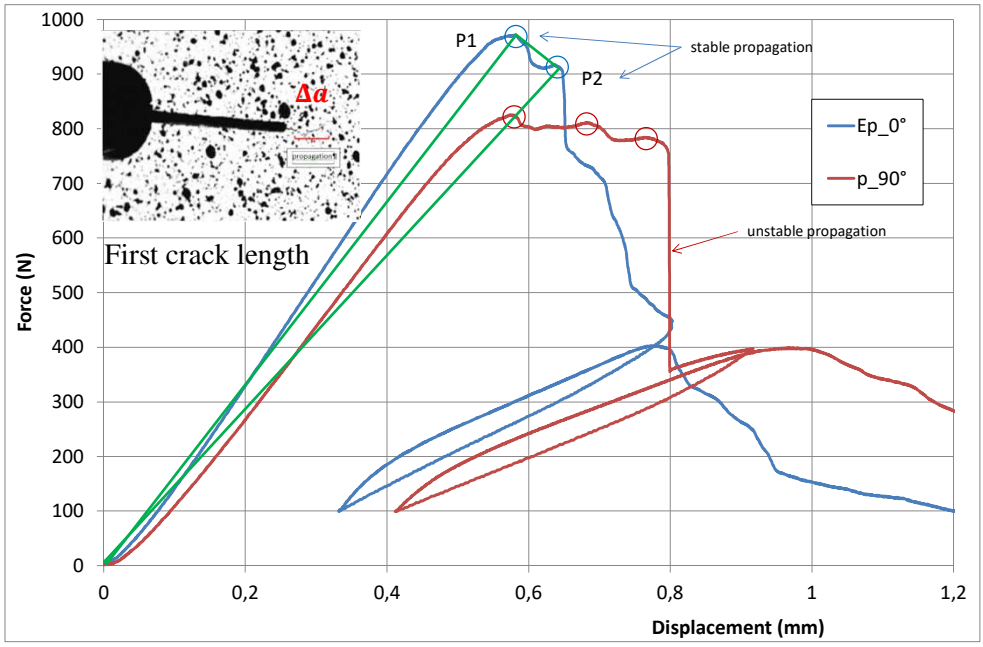

Figure 15. CT sample dimensions (a) and tensile test configuration with DIC measurement (b)

Four tests have been achieved. Results are summarized in Table 5. For the epoxy matrix, the critical energy release rate value is obtained from the literature [36, 37, 38].

Table 5. Failure energy of Flax/epoxy woven 2x2 twill ply

Gf (0° warp) J/m2	Gf (90° weft) J/m2	Gm (Matrix) J/m2
5.0 ±0.23	4.86 ±0.32	0.125

3.4. Model validation and experimental comparison

Once identified on 2x2 twill flax woven laminates, parameters and properties of the material model are introduced into a developed user material subroutine (UMAT) developed for implicit Abaqus® Software. For the purpose of validation of the model, some preliminary tests have been done with a single fully integrated solid element (8 nodes, 3 degrees of freedom per node and 8 Gauss integration points – C3D8 reference in Abaqus software). The static general solver (Quasi static implicit algorithm, Newton-Rahpson) is used in Abaqus. Displacements are prescribed at the boundaries for tensile and shear tests.

For the numerical/experimental tensile test comparison, Figure 16 shows the FE model used. Tabs are not meshed. Solid elements used are the same as prescribed before (C3D8). First section is fixed. Displacement is imposed on a reference point linked to the second section of the sample. Size of brick elements is 1.5mm×1.5mm×1.25mm. Stress-strain curves are saved for some elements situated in the middle of the sample (near strain sensors position).

The FE model results are compared to the experimental ones on Figure 16 for the two staking sequences $[0°]_4$ and $[\pm 45°]_4$. In both cases, the model is in good accordance with the experimental results.

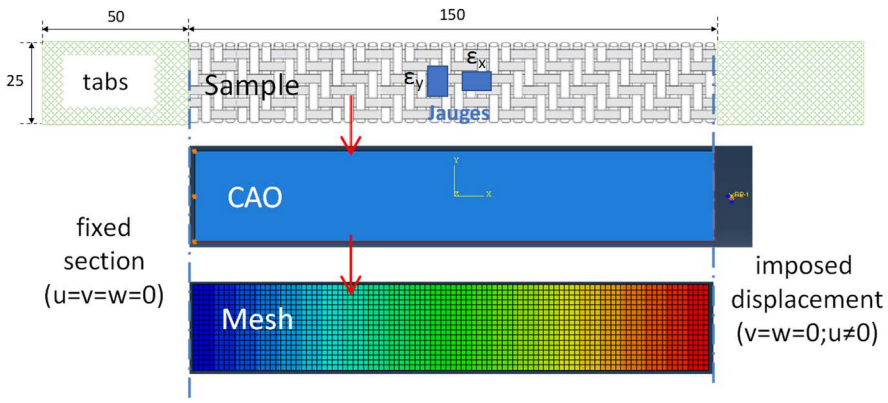

Figure 16. Mesh and boundary conditions of tensile test.

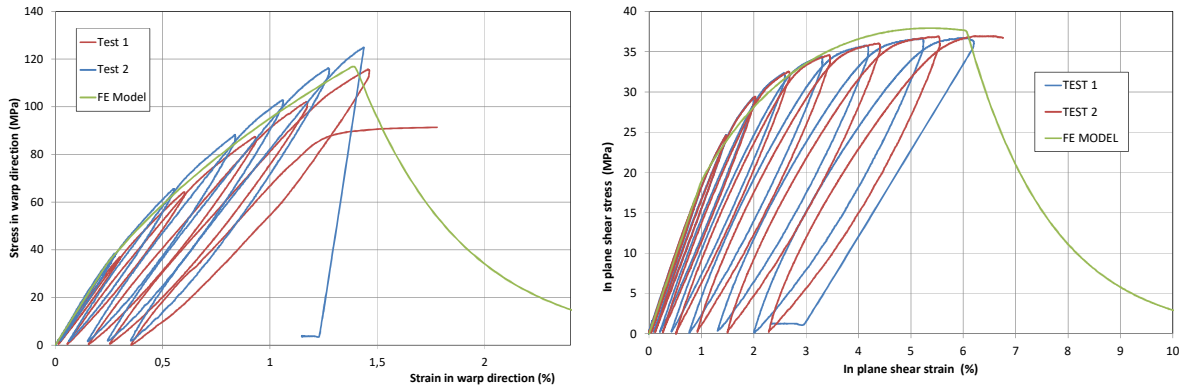

a) b)

Figure 17: Comparison of experimental and numerical FE results for $[0°]_4$ a) and $[\pm 45°]_4$ b) laminates

4. Failure prediction of omega sandwich panels

Objective of this part is to apply the damage/failure model to predict the failure modes of the Omega sandwich panel submitted to 3 points bending tests (section 2).

4.1. Mesh, boundary conditions and loading

This subsection is intended to present the model which was realized in ABAQUS in order to simulate the three point bending test. Showing the FEM model will also be a way to introduce the geometry and characteristics of the real model and also some test parameters. The real

model was built with some measure specifications, regarding the length, width and the geometry and also measures of the cross section. All the dimensions are resumed in Table 6.

Table 6: Dimension of the Omega Sandwich

Measures	lenght	width	height	Thickness of the skins	Thickness of the core
Value (mm)	200	80	11.27	0.5	0.6

This model Figure 17 has been meshed with C3D8 brick elements (Mesh obtains with a global convergence normal stress due to bending). Size of elements in skin and core part is near 1.0mm×1.0mm×0.25mm. Some elements are smaller in refined part close to rounded corners (about 0.25mm×0.25mm×0.25mm). The model tested consist on a corrugated panel, with a cross-section "*W* " shape, which can also be called omega panel (Figure 17). Two models have been created: one with skin tie to the Omega core (same nodes), other with cohesive contact including bilinear cohesive behavior. The rollers fixed use rigid element (R3D4 Abaqus reference). Imposed displacement is done on the central rectangular roller as on the experimental setup. The boundary conditions have been set with a hard contact with friction between the panel and the cylindrical/rectangular rollers.

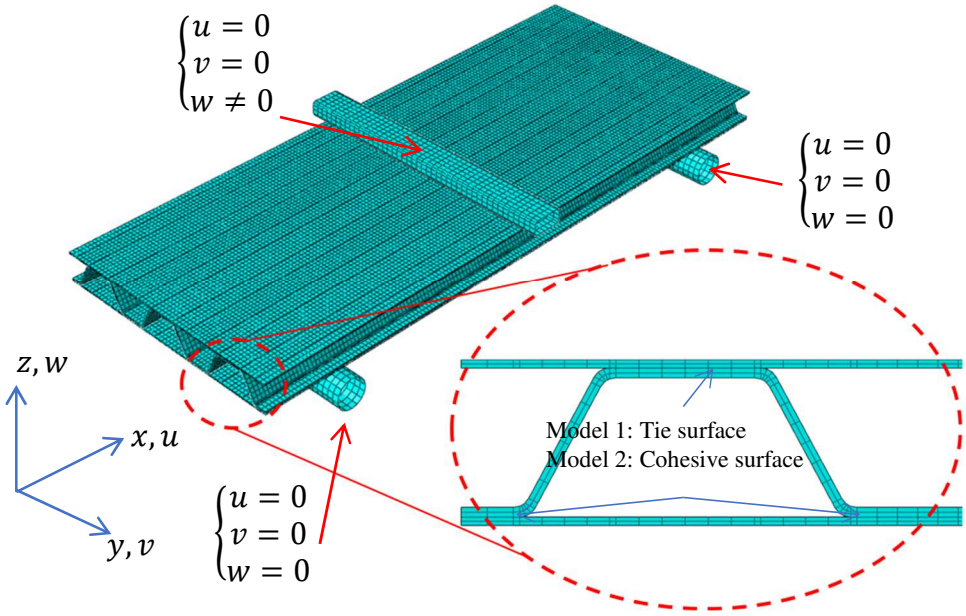

Figure 18: Mesh and boundary conditions of 3 points bending test.

4.2. Computation and input data

The computation uses the Full Newton Raphson solver (ABAQUS General Standard) with nonlinear geometric activation. The full Newton Raphson scheme involved an update of the tangent stiffness matrix at each iteration; this scheme appears to the authors as a suitable approach to support the progressive failure of laminates.

Finally a delayed damage effect [39-40] is applied to all failure damages in order to limit the localization of the damage in the model and to minimize the mesh dependency. Viscous damage is chosen as follow [41]:

$$\dot{d}_v = \frac{1}{\eta}(d_0 - d_v) \qquad \textit{Eq. 18}$$

where: d_0 is the damage variable without delay damage effect, d_v is the regularized viscous damage variable and η is a viscosity constant. τ is equal 0.0025 for all the failure damages. So

$$d_v(t+1) = \frac{\Delta t}{\eta+\Delta t} d_v(t) + \frac{\eta}{\eta+\Delta t} d(t) \qquad \textit{Eq. 19}$$

Expression of this parameter also facilitates the computation of the tangent matrix [41].

All the model input data are summarized in Table 7 for elastic ply properties, Table 8 for diffuse damage computation and Table 9 for failure characteristics. Pseudo plasticity is not activated for these computations. Model data for cohesive behaviour are given in Table 11.

Table 7: woven ply characteristics

$E_{11}=E_{22}$ (MPa)	E_{33} (MPa)	G_{12} (MPa)	$G_{13}=G_{23}$ (MPa)	ν12	ν13=ν23
17500±42	7500±62	1900±20	1600±30	0.06±0,005	0.06±0.007

Table 8: Initial values for diffuse damage computation

$\varepsilon_{11}=\varepsilon_{22}$ init (%)	ε_{33} init (%)	γ_{12} init (%)	$\gamma_{13}=\gamma_{23}$ (%)	Yf init (J/m^3)	Ym init (J/m^3)
0.23±0.05	0.52±0.025	0.63±0.035	0.85±0.045	0.5,e,E,e	0.5.g.G12.g

Table 9: Failure values for failure damage computation

$\varepsilon_{11}=\varepsilon_{22}$ fail (%)	ε_{33}fail (%)	γ_{12}fail (%)	$\gamma_{13}=\gamma_{23}$ fail (%)	Gf fail (J/m^2)	Gm fail (J/m^2)
1.45±0.12	3.45±0,.6	7.2±0.43	8.3±0.8	5000 ±163	125 ±15

Table 10: Cohesive values for cohesive behaviour

$K_{nn} = K_{nn} = K_{nn}$ (N/mm^3)	σ_{33} init (MPa)	$\sigma_{13}= \sigma_{23}$ (MPa)	GIc (J/m^2)	GIIc = GIIc (J/m^2)
100 000	50	70	125 ±15	350 ±36

4.3. Test and numerical behaviour comparison

We observed during the experimental study, two modes of failure of the panels; one by failure of the lower skin in tension, the other by debonding of the upper skin in compression (see section 2). According to these results, two types of models were analysed in a global way but also in terms of local damages.

4.3.1. Ply damage model results

The first experimental/numerical comparison uses a pure damage/failure model without cohesive behaviour. Figure 18 shows numerical/experimental comparison of load-displacement behaviours. Characteristic values as stiffness values (measured between 100N and 500N), or forces and displacements at failure, are reported in Table 11. As can be seen, the FE model simulates accurately the behaviour of the flax fibres omega panel in three point bending. The behaviour is globally nonlinear as observed experimentally and specific values in Table 11 are also very close.

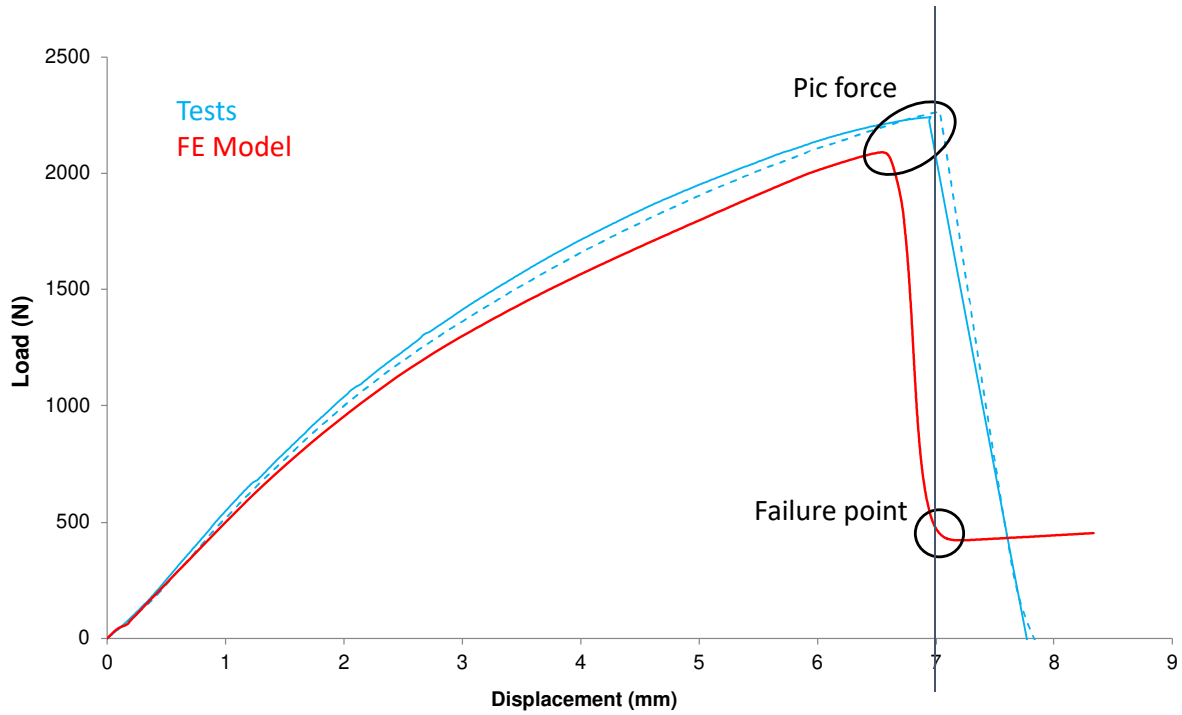

Figure 19: Numerical/Experimental load displacement behaviour comparison

Table 11: Global numerical/experimental values results comparison

	Stiffness K (N/mm)	Failure force (N)	Displacement at failure (mm)
Exp.	577	2250	7.0
FE model	528	2090	6.6
Difference	9.3 (%)	7.6 (%)	6.0(%)

Considering the failure damage, a general view of the damage in the panel at the pic force is presented in Figure 19. These pictures show that failure damage is mainly located in the lower skin in the warp direction (Figure 19-A) and initiated in the free border of the panel. Failure damages in weft direction (Figure 19-B) are located in the upper skin of the panel, and on either side of the Omega core (stiffener). In plane shear failure damage initiates only between the lower skin and the Omega core, near the border of the panel (Figure 19-C).

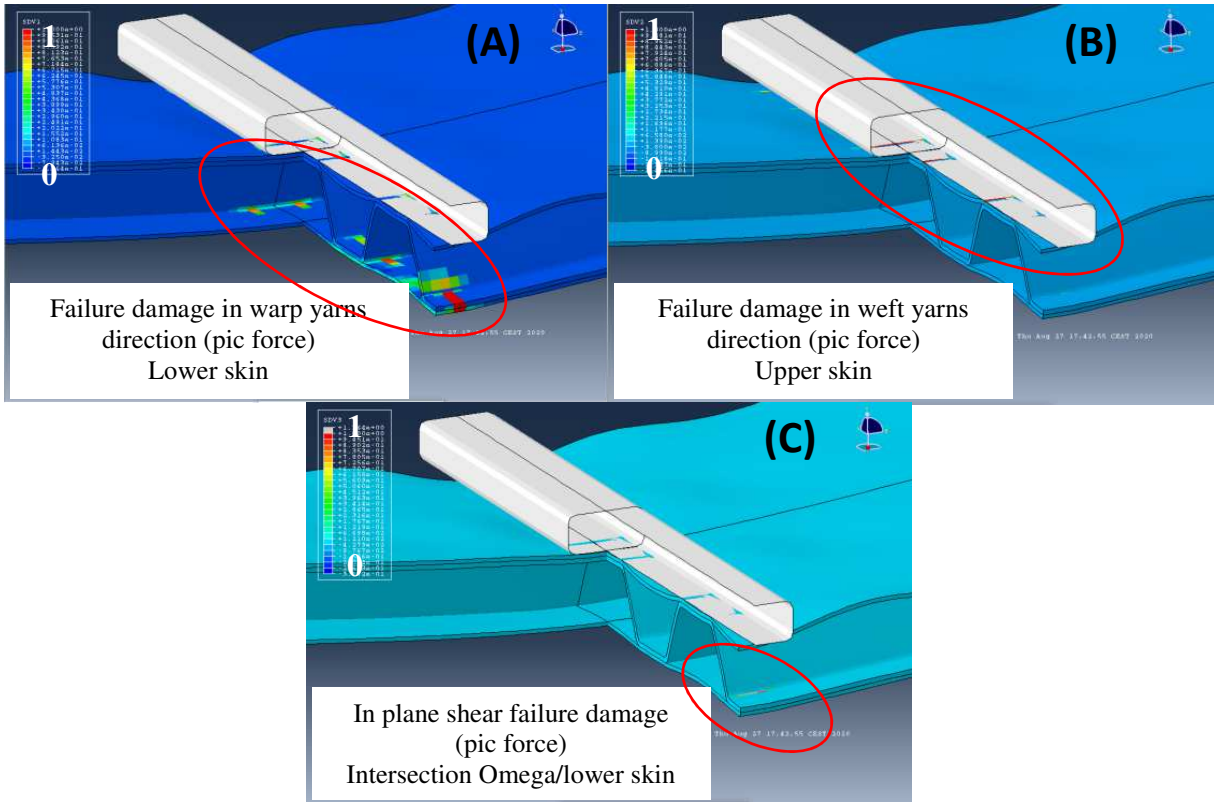

Figure 20: Position of failure damages at pic force. A) warp direction B) weft direction, C) in plane direction

Concerning the final failure mode, FE model prediction is in good accordance with experimental observations (Figure 20-B). The FE model final failure consists of two macro cracks located on either side of the rectangular central support dues to symmetry of the model. Obviously the failure observed experimentally can only consist of one single crack.

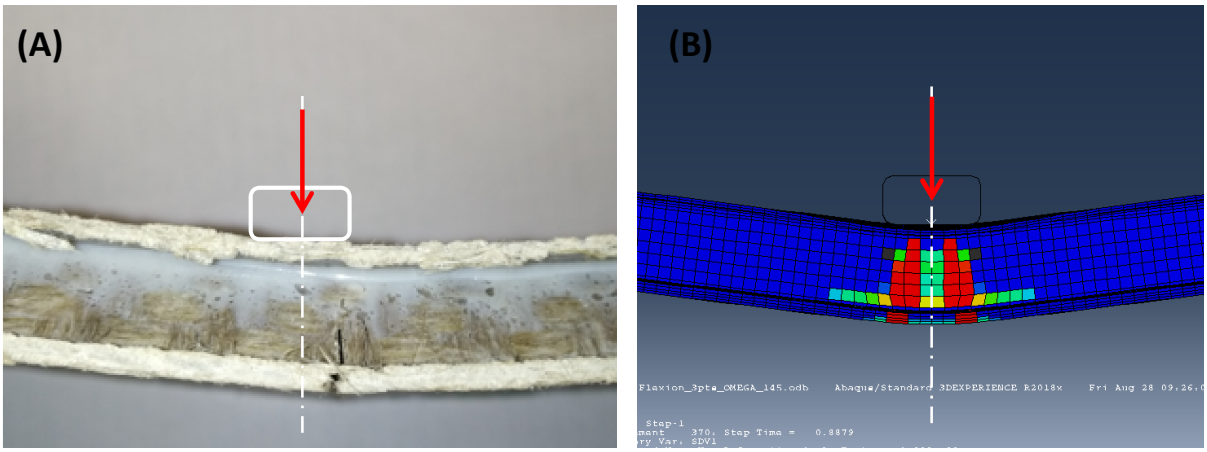

Figure 21: Numerical(B)/Experimental(A) final failure mode comparison (B shows warp damage failure values)

So the first failure mode is well predicted. Secondly, the model includes cohesive behaviour and damage/failure of woven plies.

4.3.2. Damage/Failure with skin debonding approach

A model integrating classical cohesive damage behaviour [38] between the Omega core and the skins was created in order to simulate the failure mode 2 with the buckling of the upper skin. The cohesive zone model (CZM) uses a bi-linear behaviour described by Lachaud [38]. Quadratic stress criterion is used of initiation of delamination. A linear propagation energy criterion is defined. Figure 19 shows experimental/numerical global load-displacement behaviours. Specific characteristics values as stiffness values, pic loads and failure displacements are shown in Table 12. It can be seen that in this configuration as well, the FE model is capable to describe the non-linear behaviour of the panel until the failure load is reached. Up to this point, specific values of stiffness and maximum load are very close (Table 12).

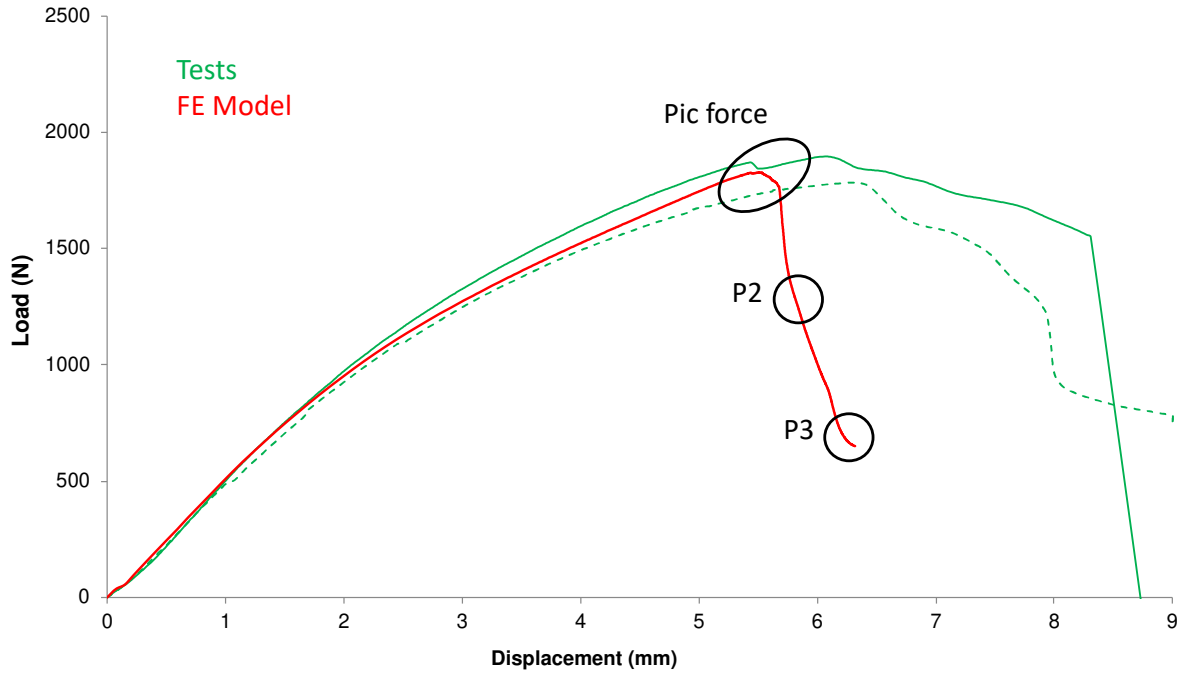

Figure 22: Numerical/Experimental load displacement behaviour comparison. Model with cohesive behaviour and ply damage/failure model

Table 12: Global numerical/experimental values results comparison

	Stiffness K (N/mm)	Failure force (N)	Displacement at failure (mm)
Exp.	577	1845	6,3
FE model	533	1820	5.6
Difference	8.2 (%)	5.6 (%)	12.5 (%)

The general view of the cohesive damage at different relevant steps of the failure is presented in Figure 22. These three steps correspond to the three points showed in Figure 21. We can see that debonding is initiated at each corner of the upper side of the Omega stiffeners, under the central rectangular roller (Figure 23-A). After reaching the full width of the omega top faces, debonding then propagates in the longitudinal direction of the samples (Figure 23-B). When debonding of the upper skin is sufficiently important, local buckling arises (Figure 22-C).

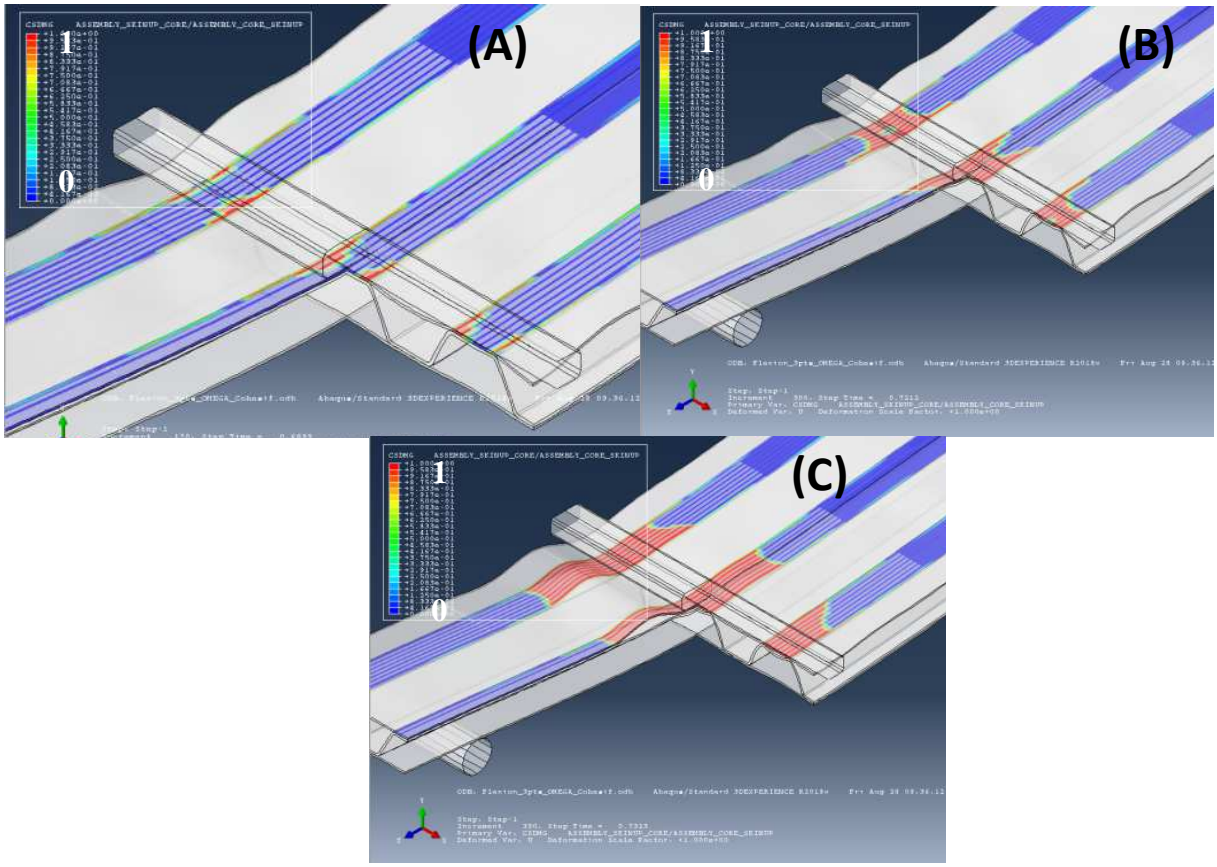

Figure 23: Cohesive damage parameter during softening part of the 3 points bending behaviour A) pic force, B) longitudinal propagation of debonding and C) local buckling

The final failure of the panel obtained by the FE model with cohesive behaviour is compared with the experimental one on Figure 23. Debonding of the upper skin is very similar to that obtained experimentally. So the second failure mode is well predicted.

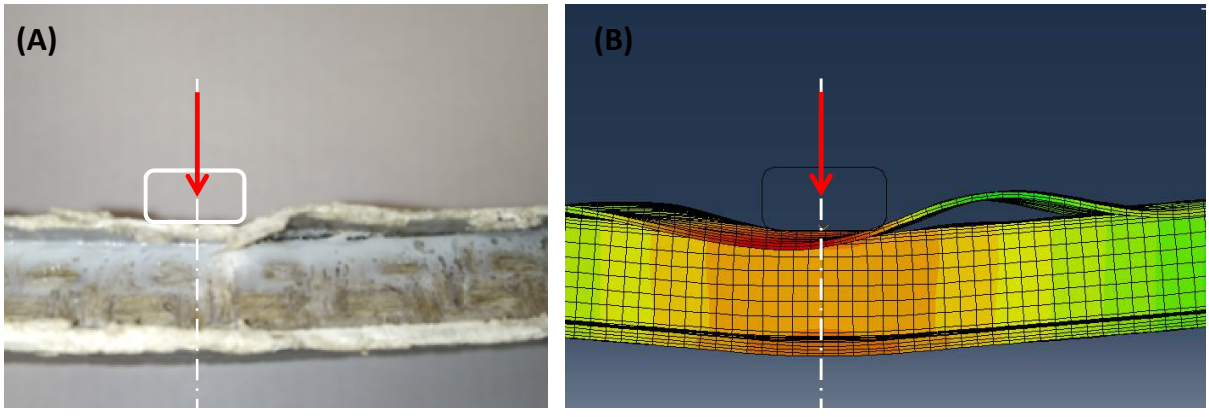

Figure 24: Experimental(A) /numerical(B) final failure mode by Core/Skin debonding (B shows displacement values)

The model is not able to take into account failure mode I while mode I will appear. Local bonding defects or geometric defects during manufacturing can be the initiators of the two observed failure modes.

5. Conclusion

The main goal of the study was to study multi-scale mechanical behaviour of composite flax fibres reinforced polymer composites, in order to evaluate of this type of material could be used in aeronautical structures. A new manufacturing process of a flax woven ply sandwich panel was developed with Omega stiffeners by hand manufacturing with high pressure curing.

Global behaviour of Flax Omega sandwich panels were compared with some conventional sandwich panels made of a woven glass skin with NOMEX core under static three point bending loading. It appears that the flax fibre sandwich panels have a more marked non-linear behaviour than the Nomex sandwich panels. However, the failure force level of all the panels is similar, with a higher deformation at failure. Moreover, the panels exhibited similar mechanical properties as classical glass fibres reinforced polymer composite panels used in aeronautics.

Two failure modes of the Flax panel have been identified and observed after the tests. The first one is a tensile failure of the lower skin of the panel. The second one is a debonding and buckling of the upper skin of the panel.

The nonlinear behaviour of Omega panels has been attributed to the strong nonlinearity of the flax fibres behaviour in yarn direction, and possible defects in the panel assembly. This is why a ply damage/failure model behaviour has been proposed. This four phase model introduces a linear part followed by non-linear phases: damage model follows a

thermodynamic approach; a failure model is based on strain failure criterion coupled with the energy release rate. After presenting the material model, the identification procedure has been detailed. The model has been developed as a user material model subroutine in Abaqus standard software for non-linear static analyses. An experimental versus numerical comparison of the ply behaviour has been presented which show a very good agreement.

This model has been used to predict the global and local behaviour including damage failure and debonding of Flax Omega sandwich panels using a 3D FE model. This model has been proved to be able to predict the global non-linear force-displacement behaviour of the Omega Flax Sandwich Panel and also the local failure modes observed experimentally. The first one is due to tensile failure of the lower skin of the panel. The second one is due to debonding of the upper skin probably due to the presence of bonding defects of the skin, observed on some panels.

These results are promising for the use of flax fibre composites in aeronautical structures as a replacement solution of glass fibre composite sandwich panels.

This study could be extended in various ways like using a bio-base matrix that could be modified in order to pass aeronautics norms, especially for fire resistance. It could also be considered to use this model to optimize the structure of the omega or to perform some dynamic analysis such as impact tests or modal analysis.

6. Acknowledgement

The research leading to these results has received funding from ADEME under the grant agreement n° 1501C0050. Thesis of Mathieu BOUTIN was partially funded by ANRT (National Association of Research and Technology). The authors would like to sincerely thank Robert PIQUET, who died on March 20, 2020 for his initial contribution in this study.

7. Bibliography

[1] Baley C and Bourmaud A 2014 Average tensile properties of French elementary flax fibres Mater. Lett. 122 159–61

[2] Lefeuvre A, Bourmaud A, Lebrun L, Morvan C and Baley C 2013 A study of the yearly reproducibility of flax fibre tensile properties Ind. Crops Prod. 50 400–7

[3] Wambua, P., Ivens, J., Verpoest, I., 2003. Natural fibres: Can they replace glass in fibre reinforced plastics? Composites Science and Technology, Vol. 63 (9), pp. 1259-1264.

[4] Riccio, A., Raimondo, A., Saputo, S., Sellitto, A., Battaglia, M., Petrone, G., 2018. A numerical study on the impact behaviour of natural fibres made honeycomb cores. Composite Structures, Vol. 202, pp. 909-916.

[5] Pickering K L, Efendy M G A and Le T M 2016 A review of recent developments in natural fibre composites and their mechanical performance Compos. Part Appl. Sci. Manuf. 83 98–112

[6] Lefeuvre A, Bourmaud A, Morvan C and Baley C 2014 Tensile properties of elementary fibres of flax and glass: Analysis of reproducibility and scattering Mater. Lett. 130 289–91

[7] Pucci M F, Liotier P-J, Seveno D, Fuentes C, Van Vuure A and Drapier S 2017 Wetting and swelling property modifications of elementary flax fibres and their effects on the Liquid Composite Molding process Compos. Part Appl. Sci. Manuf. 97 31–40

[8] Fuentes C A, Brughmans G, Tran L Q N, Dupont-Gillain C, Verpoest I and Van Vuure A W 2015 Mechanical behaviour and practical adhesion at a bamboo composite interface: Physical adhesion and mechanical interlocking Compos. Sci. Technol. 109 40–7

[9] Tran L Q N, Fuentes C A, Dupont-Gillain C, Van Vuure A W and Verpoest I 2013 Understanding the interfacial compatibility and adhesion of natural coir fibre thermoplastic composites Compos. Sci. Technol. 80 23–30

[10] Faruk O, Bledzki A K, Fink H-P and Sain M 2012 Biocomposites reinforced with natural fibres: 2000–2010 Prog. Polym. Sci. 37 1552–96

[11] Kabir M M, Wang H, Lau K T and Cardona F 2012 Chemical treatments on plant-based natural fibre reinforced polymer composites: An overview Compos. Part B Eng. 43 2883–92

[12] Gopalakrishnan P, Saiah R, Gattin R and Saiter J M 2008 Effect of mercerization of flax fibres on wheat flour/flax fibre biocomposite with respect to thermal and tensile properties Compos. Interfaces 15 759–70

[13] Balnois E, Busnel F, Baley C and Grohens Y 2007 An AFM study of the effect of chemical treatments on the surface microstructure and adhesion properties of flax fibres Compos. Interfaces 14 715–31

[14] Pizzi A, Kueny R, Lecoanet F, Massetau B, Carpentier D, Krebs A, Loiseau F, Molina S and Ragoubi M 2009 High resin content natural matrix–natural fibre biocomposites Ind. Crops Prod. 30 235–40

[15] Gouanve F, Meyer M, Grenet J, Marais S, Poncin-Epaillard F and Saiter J-M 2006 Unsaturated polyester resin (UPR) reinforced with flax fibres, untreated and cold He plasma-treated: thermal, mechanical and DMA studies Compos. Interfaces 13 355–64

[16] Acera Fernández J, Le Moigne N, Caro-Bretelle A S, El Hage R, Le Duc A, Lozachmeur M, Bono P and Bergeret A 2016 Role of flax cell wall components on the microstructure and transverse mechanical behaviour of flax fabrics reinforced epoxy biocomposites Ind. Crops Prod. 85 93–108

[17] Arnould O, Siniscalco D, Bourmaud A, Le Duigou A and Baley C 2017 Better insight into the nano-mechanical properties of flax fibre cell walls Ind. Crops Prod. 97 224–8

[18] Bourmaud A, Morvan C, Bouali A, Placet V, Perré P and Baley C 2013 Relationships between micro-fibrillar angle, mechanical properties and biochemical composition of flax fibres Ind. Crops Prod. 44 343–51

[19] Baley C 2004 Influence of kink bands on the tensile strength of flax fibres J. Mater. Sci. 39 331–334

[20] Baley, C., 2002. Analysis of the flax fibres tensile behaviour and analysis of the tensile stiffness increase Composites - Part A: Applied Science and Manufacturing, Vol. 33 (7), pp. 939-948.

[21] Mahboob Z, El Sawi I, Zdero R, Fawaz Z and Bougherara H 2017 Tensile and compressive damaged response in Flax fibre reinforced epoxy composites Compos. Part Appl. Sci. Manuf. 92 118–33

[22] Mahi A E, Daoud H, Rebiere J-L, Gimenez I, Taktak M and Haddar M 2019 Damage mechanisms characterization of flax fibres–reinforced composites with interleaved natural viscoelastic layer using acoustic emission analysis J. Compos. Mater. 53 2623–37

[23] Sun C T and Vaidya R S 1996 Prediction of composite properties from a representative volume element Compos. Sci. Technol. 56 171–9

[24] Thuault A, Bazin J, Eve S, Bréard J and Gomina M 2014 Numerical study of the influence of structural and mechanical parameters on the tensile mechanical behaviour of flax fibres J. Ind. Text. 44 22–39

[25] Beakou A and Charlet K 2013 Mechanical properties of interfaces within a flax bundle—Part II: Numerical analysis Int. J. Adhes. Adhes. 43 54–9

[26] Tephany C, Soulat D, Gillibert J and Ouagne P 2016 Influence of the non-linearity of fabric tensile behaviour for preforming modeling of a woven flax fabric Text. Res. J. 86 604–17

[27] Sliseris J, Yan L and Kasal B 2016 Numerical modelling of flax short fibre reinforced and flax fibre fabric reinforced polymer composites Compos. Part B Eng. 89 143–54

[28] Wang W, Lowe A, Davey S, Akhavan Zanjani N and Kalyanasundaram S 2015 Establishing a new Forming Limit Curve for a flax fibre reinforced polypropylene composite through stretch forming experiments Compos. Part Appl. Sci. Manuf. 77 114–23

[29] Panamoottil S M, Das R and Jayaraman K 2016 Anisotropic continuum damage model for prediction of failure in flax/polypropylene fabric composites Polym. Compos. 37 2588–97

[30] Sellitto, A., Riccio, A., Russo, A., Zarrelli, M., Toscano, C., Lopresto, V., 2019. Compressive behaviour of a damaged omega stiffened panel: Damage detection and numerical analysis. Composite Structures, Vol. 209, pp. 300-316.

[31] Mahboob Z., Bougherara H., 2018, Fatigue of flax-epoxy and other plant fibre composites: critical review and analysis. Composite Part A., Vol 109, 440-462

[32] Ladeveze P and Ledantec E 1992 Damage modelling of the elementary ply for laminated composites Compos. Sci. Technol. 43 257–67

[33] Linde P, Pleitner J, de Boer H and Carmone C 2004 Modelling and Simulation of Fibre Metal Laminates. Materials Science. Corpus ID: 55309277

[34] Pinho S. T., Robinson P., Iannucci L. 2006 Facture toughness of the tensile and compressive fibre failure modes in laminated composites. Composite Sciences and Technology, Vol. 66, Issue 13, october 2006, pages 2069-2079.

[35] Médeau V., Laurin F., Rannou J., Hurmane A., Quillent H, Lachaud F. 2019. Robust characterization of crack propagation in 3D woven composites and evidences of size dependency. Composite Structures. Vol. 225, 1 october 2019,111175.

[36] Lachaud F., Lorrain B., Michel L., Barriol R. 1998 Experimental and numerical study of delamination caused by local buckling of thermoplastic and thermoset composites. Composite Science and Technology. 03-1998.

[37] Lubineau G, Ladeveze P. 2008. Construction of a michromechanics-based intralaminar mesomodel, and illustrations in Abaqus/Standard. Computational Materials Science, Vol. 43, pp 137-145.

[38] Lachaud F, Paroissien E and Michel L 2020 Validation of a simplified analysis for the simulation of delamination of CFRP composite laminated materials under pure mode I Compos. Struct. 237 111897

[39] Allix O. and Deü J.-F., 1997. Delayed damage modelling for fracture prediction of laminated composites under dynamic loading, Engineering Transactions, vol. 45, no. 1, pp. 29–46.

[40] Montagne B., Lachaud F., Paroissien E., Martinie D., and Congourdeau F., 2020. Failure analysis of single lap composite laminate bolted joints : Comparison of experimental and numerical tests. Composite Structures, Vol 236, 111949.

[41] Chen JF, Morozov EV, Shankar K., 2012. A combined elastoplastic damage model for progressive failure analysis of composite materials and structures. Composite Structures, Vol. 94(12):99. 3478–89.